33rd Annual International Conference of the IEEE EMBS
Boston, Massachusetts USA, August 30 - September 3, 2011

A Transparent µECoG Array for Simultaneous Recording and Optogenetic Stimulation

Peter Ledochowitsch, Elisa Olivero, Tim Blanche, and Michel M. Maharbiz, *Member, IEEE*

***Abstract*—In this paper we report for the first time the design, fabrication and characterization of an optically transparent electrode array for micro-electrocorticography. We present a 49-channel µECoG array with an electrode pitch of 800 µm and a 16-channel linear µECoG array with an electrode pitch of 200 µm. The backing material was Parylene C. Transparent, sputtered indium tin oxide (ITO) was used in conjunction with e-beam evaporated gold to fabricate the electrodes. We provide electrochemical impedance characterization and light transmission data for the fabricated devices.**

I. Introduction

STATE of the art tools for simultaneous optogenetic stimulation and electrophysiological recordings, such as 'optrodes' [1], are invasive and can cover only a very small fraction of the cortex with relatively few stimulation and recording sites. The importance of electrocorticography (ECoG) -- the measurement of electrical potentials on the surface of the cerebral cortex -- is growing for both brain-machine-interfaces (BMI) and as a fundamental research tool for the investigation of long-range neural circuitry and synchronization [2,3]. In this paper, we present an optically transparent µECoG array, which allows optical stimulation of neural tissue immediately beneath the array (Fig. 1).

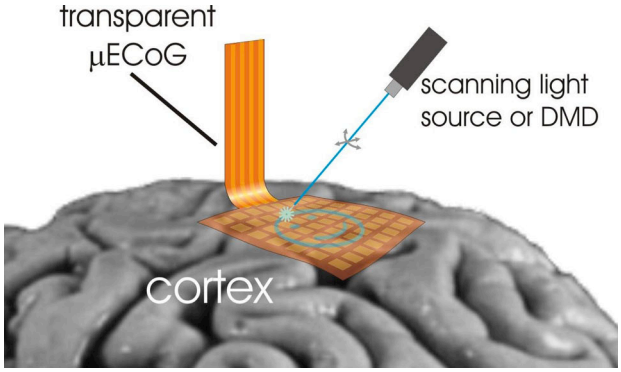

Fig. 1. Integration of µECoG with optogenetics. Patterned light, e.g. from a Digital Micromirror Device (DMD), excites transfected or transgenic neural tissue underneath a transparent µECoG array. Electrical activity detected by the µECoG could be feedback-coupled with the light-source output to control activation states on the cerebral cortex.

Manuscript received April 18, 2011. This work was supported by member fees of the Berkeley Sensors and Actuators Center (BSAC) and by NIH-5R21NS066260.

P. Ledochowitsch is with the Bioengineering Department, University of California, Berkeley, CA 94720 USA, (corresponding e-mail: pledoch@eecs.berkeley.edu).

E. Olivero is a visiting scholar at EECS department, University of California, Berkeley, CA 94720 USA from the Polytechnic of Turin, Turin, Italy.

T. Blanche is with the Redwood Center for Theoretical Neuroscience and the Helen Wills Neuroscience Institute, University of California, Berkeley, CA 94720 USA.

M. M. Maharbiz is a professor of Electrical Engineering and Computer Science, University of California, Berkeley, CA 94720 USA.

ECoG constitutes a trade-off in invasiveness and spatial resolution between traditional scalp electroencephalography (EEG) and penetrating microelectrode recordings. In the 1950's, Jasper and Penfield pioneered ECoG [4] for pre-surgical evaluation of patients suffering from intractable epilepsy. Brindley and Craggs reported a correlation between voluntary movement and ECoG signals as early as 1972 [5]. More recently, the BMI community demonstrated the great promise of ECoG-based BMIs [6] for the neural control of high performance motor [7] and communication [8] prostheses, e.g. for locked-in patients. For BMI applications, the development of large area, high-resolution ECoG grids [9,10] is key.

Neural recordings constitute only part of a larger tool kit required to 'reverse engineer' the brain (i.e. to understand its normal or pathological dynamics as properties of underlying neural circuits). Ideally, it is also desirable to trigger artificial neural signals and to study how this information is transformed in the brain. A specific example of this can be seen in BMI for motor control [10]. Successful motor control is highly dependent on proper sensory feedback. In this context, it is essential to close the motor-sensory feedback loop (for example, to integrate a prosthetic limb into a patient's proprioception) and this requires information 'write-in' [11].

Neurons can be stimulated electrically but with poor spatial resolution, and stimulation artifacts render simultaneous electrophysiological recordings at the same site very difficult. Boyden and Deisseroth recently demonstrated that neurons can be rendered sensitive to stimulation by light [12]. Neurons transfected with a light-sensitive ion channel, such as channelrhodopsin, bacteriorhodopsin and halorhodopsin, can be individually modulated to either fire or suppress action potentials when illuminated at the correct wavelength.

Integration of this powerful new stimulation approach with ECoG requires the development of a transparent, flexible, and biocompatible electrode array. The fabrication of flexible transparent electrodes has to date been mainly developed for LEDs, flexible displays and solar cells. Several materials and deposition methods have been investigated to achieve the best tradeoff between transparency and conductivity. Transparent conductive oxides (TCOs) such as indium tin oxide (ITO) can be found in numerous industrial applications due to their high electrical conductivity and transparency over the entire visible spectrum [13]. However, ITO is a relatively brittle ceramic material and thus it is considered suboptimal for flexible electrodes [14]. While alternatives such as single walled carbon nanotube percolation networks [15], silver

nanowire percolation networks [16] and graphene layers [17] are being investigated, ITO is a material with superior conductivity, transparency and biocompatibility [18], and is easily sputtered and patterned lithographically.

In preliminary experiments we fabricated an ECoG array using ITO as the conductor for all electrodes in the array but the large bond pads broke along stress lines at the edge of plasma-etched vias (Fig. 4a). Interestingly, ITO microelectrode pads and buried traces remained intact. In this paper, we mitigate the brittleness of ITO by confining it to the microelectrodes and to short pieces of buried interconnect traces while the long interconnect traces and bonding pads are fabricated out of ductile gold.

II. Design

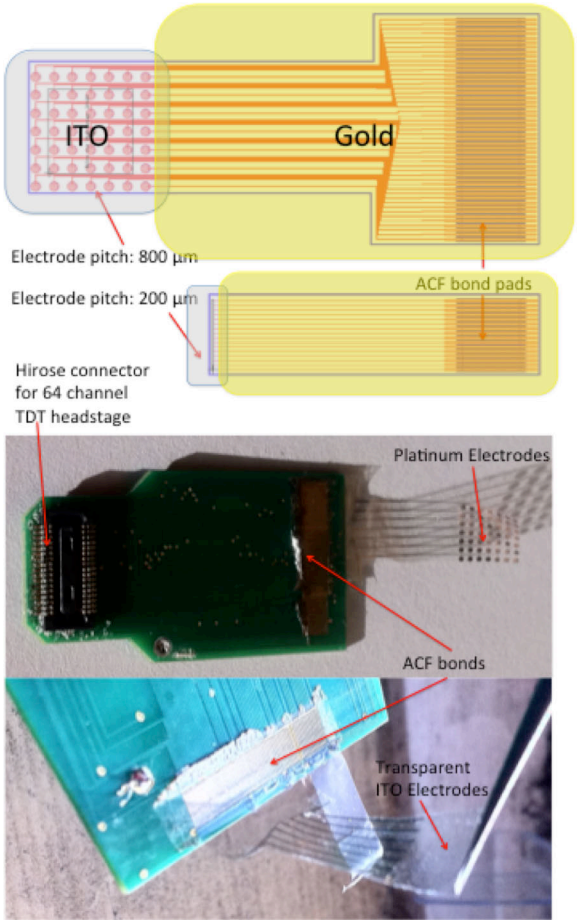

Fig. 2. Top: ECoG CAD designs (49 channel 2D array with 800 µm pitch and 16 channel linear array with 200 µm pitch). Bottom left: Baseline (Cr/Au/Pt stack) ECoG. Bottom right: Hybrid Au-ITO ECoG.

We have designed a 49-channel µECoG array with an electrode pitch of 800 µm and a 16-channel linear µECoG with an electrode pitch of 200 µm (Fig. 2). A 2 cm long Parylene cable was monolithically integrated with the ECoG array at the wafer level. In our prototype devices all conductors were formed by a tri-stack of chrome (10 nm Cr), gold (200 nm Au) and platinum (50 nm Pt). In the hybrid Au-ITO devices the linear bond pad array (pad dimensions: 100 µm × 2500 µm, 200 µm pitch) and most of the conductor traces (width: 20 µm) consisted of Cr/Au (10 nm / 100 nm). However, near the microelectrode array gold overlapped with ITO (110 nm) and the electrodes were made entirely of ITO to achieve transparency (blue shaded regions in Fig. 2).

The cable was thermo-compression-bonded to a fan-out printed circuit board (PCB) in an anisotropic conductive film (ACF) bonding process. The adaptor PCB was outfitted with two 34-pin ZIF connectors (DF30FC-34DS-0.4V, Hirose) compatible with the *ZIF-Clip*® neural recording headstage amplifiers made by Tucker Davis Technologies (TDT).

The choice of biocompatible materials and the form factor of our devices allow for acute and chronic application in rodent, feline, non-human primate and in human subjects.

III. Fabrication

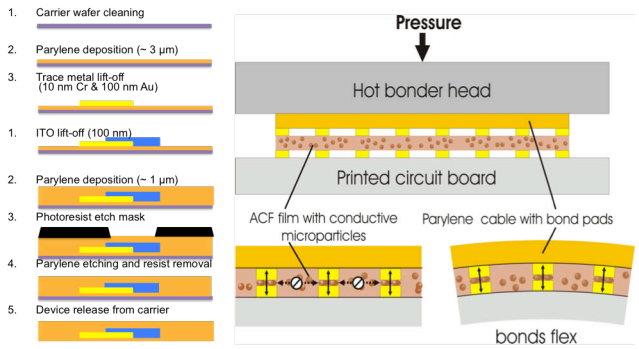

Fig. 3. Fabrication and assembly. Left: Au-ITO hybrid device fabrication process. Top right: The ACF film is thermo-compressed between complementary pad arrays. Top middle: Au-coated polymer microspheres embedded in the epoxy establish a robust electrical connection. Between adjacent pads the microparticles remain surrounded by insulating polymer that prevents shorts. Bottom right: The cured epoxy provides mechanical stability under flexion.

A. Waferlevel Fabrication

The wafer-level fabrication process is shown in Fig. 3 (left). A 3 µm thick layer of Parylene C (poly(para-chloro-xylylene) layer was deposited on a 4'' silicon carrier wafer using a (Specialty Coating Systems) Parylene System Model 2010 under conditions shown in Table 1. Enclosing the wafer holder inside an ultra-fine stainless steel mesh (McNichols, square weave, stainless steel type 304, 325 mesh, 0.0014" Wire, 0.0017" opening) was key to avoiding particulate contamination during parylene deposition.

Table. 1. Parylene C deposition parameters per Marvell Nanolab manual: http://nanolab.berkeley.edu/labmanual/chap6/6.22parylene.pdf.

$T_{furnace}$ [°C]	$T_{chamber}$ [°C]	$T_{vaporizer}$ [°C]	$P_{chamber}$ [mTorr]	Mass [g]
360	57	80	25	3

The conductor was patterned in a bi-layer lift-off process. A 1.3 µm thick layer of G-line resist (OCG 825) was spun at 5000 RPM on top of the Parylene. The wafer was soft baked at 90 °C for 60 seconds and flood exposed (Karl Suss MA6

0.14 J/cm^2). A layer of I-line photoresist (OiR 10i 1.1 µm thick) was then spun at 4100 RPM and soft baked at 90 °C. The wafer was exposed with a dose of 0.06 J/cm^2 and developed in OPD 4262 for 60 s. A 20 s etch in oxygen plasma (80 sccm and 200 W RF power) was performed in the Plasma-Therm PK-12 RIE tool to de-scum the surface and improve adhesion for metal deposition. For the prototype devices, a tri-stack of metal (10 nm Cr / 200 nm Au / 50 nm Pt) was electron-beam (e-beam) evaporated. Fabrication of the hybrid devices required two separate deposition and lift-off steps: A stack of two metal layers (10 nm Cr / 100 nm Au) was e-beam evaporated. The metal was lifted-off by soaking in acetone for 10 min. After a second lithographic step, ITO was sputtered from an In_2O_3:SnO_2 (10 wt% SnO_2) target in Edwards Auto 306 DC and RF Sputter Coater in argon (Ar) at a pressure of 2.2 mTorr (base pressure: $4 \cdot 10^{-5}$ Torr) and a DC power density of 1 W/cm^2, yielding a 110 nm thick layer (sputter time: 33 min, deposition rate: 3.3 nm/min). Lift-off was performed followed by another de-scum etch, as described above. A thin adhesion layer of γ-MPS (γ-methacryloxypropyltrimethoxysilane) was deposited through AMST Molecular Vapor Deposition System MVD100 and another 3 µm thick Parylene layer was deposited. The vias and a device outline were patterned through two separated photolithography steps and oxygen plasma etching (200 W, 73 mTorr, 15 x 30 s intervals with 30 s cool-down period in Plasma-Therm PK-12 RIE). Finally, the devices were released from the silicon carrier wafer in a mild solution of detergent in deionized water. Micrographs and SEM images of the fabrication results are shown in Figure 4.

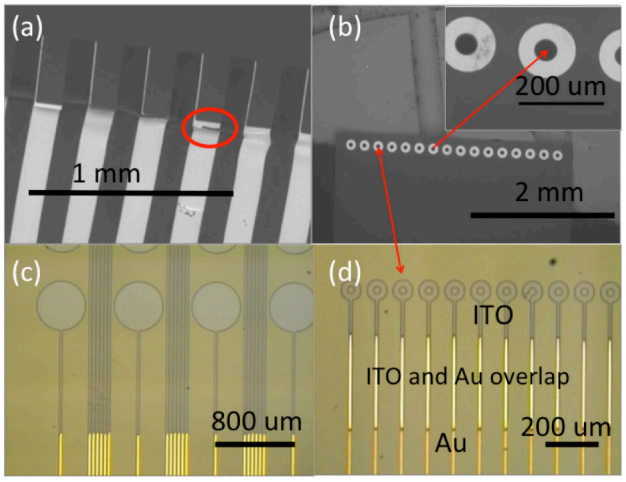

Fig. 4. Micrographs and SEM images of the 16-channel and 49-channel devices. (a) Bond pad damage on ITO-only devices. (b) Intact electrodes of a 16-channel ITO device. (c) Electrodes and interconnects of a 49-channel Au-ITO hybrid device. (d) 16-channel hybrid array. The ring-shaped electrodes are made of ITO. The light yellow lines indicate the overlap of Au and ITO. The lower part of the connections consists of Cr/Au.

B. *Assembly and Packaging*

A fan-out PCB with 3-mil-trace/space was manufactured by Sierra Circuits to connect a 1D array of ACF bonding pads (pad dimensions: 100 µm × 2500 µm, 200 µm pitch) to two footprints of surface mount Hirose connectors (DF30FC-34DS-0.4V).

The wafer level devices were bonded to the PCB in an ACF process as shown in Fig. 3 (right). ACF (3M 5552R, 2 mm wide) was pre-bonded to the corresponding PCB footprint using an Ohashi HMB-10 table-top bonder equipped with a 2.5 mm wide bond head (1 s, 90 °C, 5 kg/cm^2). Parylene devices were aligned under a stereomicroscope using a custom alignment system comprising two vacuum chucks mounted on θxyz - micropositioners, and tacked to the ACF film with a soldering iron. The final bond was performed using the HMB-10 (20 s, 200 °C, 40 kg/cm^2).

IV. Results

A. *Optical properties of ITO film*

Transparency was measured using an ellipsometer/spectrometer (Sopra GESP) under normal incidence. The transmittance, normalized with respect to the substrate, exceeded 90% over most of the visible spectrum (Fig. 5).

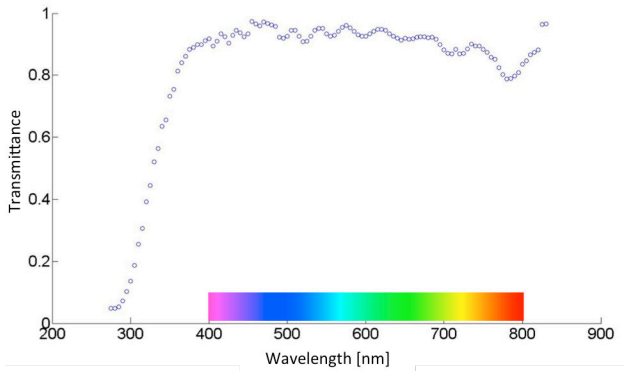

Fig. 5. Transmittance of the 110 nm thin ITO film is shown as a function of wavelength (285 nm to 830 nm).

B. *Electrical Characterization*

The sheet resistance of the ITO was determined to be 43.7 Ω/square in a 4-point-probe (VEECO FPP-5000) measurement. The resistivity was calculated to be 4.807×10^{-6} Ωm. ITO traces in our design are between 1 mm and 6.5 mm in length. Thus, from device geometry, we expected a series resistance between 2.2 kΩ and 14.2 kΩ for each electrode.

We characterized the electrode/electrolyte interface by electrochemical impedance spectroscopy (EIS) (*nanoZ*™, White Matter, LLC, frequency sweep: 5 Hz to 5 kHz). The device formed the active electrode and a silver wire formed the reference electrode. We used artificial cerebrospinal fluid (aCSF, Artificial CSF Perfusion Fluid, Harvard Apparatus, ion concentrations in mM: [Na^+] = 150; [K^+] = 3.0; [Ca^{2+}] = 1.4; [Mg^{2+}] = 0.8; [PO^{4-}] = 1.0; [Cl^-] = 155) as the electrolyte.

The data were fitted to a Randles Cell model using EIS

Spectrum Analyzer [19] to extract the line resistance $R_s = 9.36 \pm 5.53$ kΩ, charge transfer resistance $R_p = 187.29 \pm 56.17$ MΩ and the parameters of the constant phase element (CPE) parameters $n = 0.87 \pm 0.002$ and $P = 1.58 \pm 0.02$ $s^n/(\Omega cm^2)$ shown in Fig. 6. The series resistance value was in good agreement with our predictions. Approximating the CPE with a capacitor, we calculated the capacitance per area of the ITO pads to be 1.39 ± 0.02 μF cm^{-2}) which is an order of magnitude lower than that of platinum pads (60 μF cm^{-2}) [20]. The parallel resistance was expected to be very high as all testing is performed at voltages far below electrochemical potentials and no Faradaic charge transfer was expected. We calculated a pad-electrolyte interface resistance of 212 ± 60 kΩ cm^2 which was similar to values reported for platinum in literature (220 kΩ cm^2) [20].

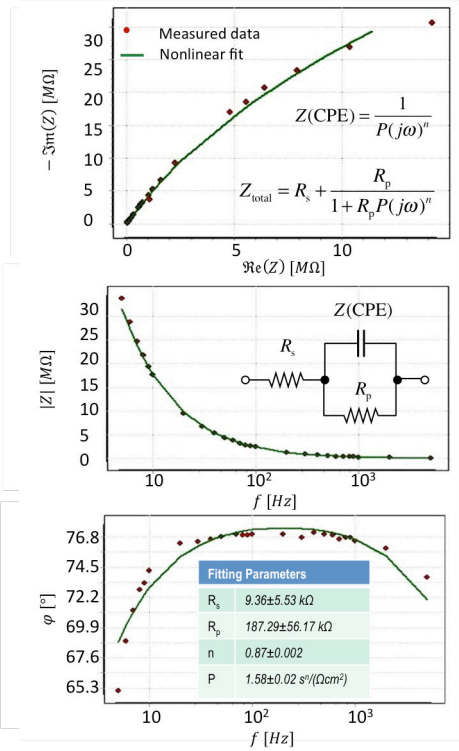

Fig. 6. Characterization of the electrode-electrolyte interface by electrochemical impedance spectroscopy. The data were adequately fit by the Randles Cell circuit model.

V. Conclusion

Conductive and transparent ITO films were successfully DC-sputtered on Parylene and patterned by lift-off. While ITO on Parylene is quite brittle, our approach successfully combined metal interconnects with ITO microelectrodes, resulting in flexible, transparent hybrid μECoGs with good electrical and excellent optical characteristics.

Acknowledgment

The authors thank Daniel Cohen for SEM imaging, the staff of the U.C. Berkeley Marvell Nanolab (http://nanolab.berkeley.edu/) and Prof. Philip N. Sabes for useful discussions.

References

[1] V. Gradinaru, K.R. Thompson, F. Zhang, M. Mogri, K. Kay, M.B. Schneider, and K. Deisseroth, "Targeting and readout strategies for fast optical neural control in vitro and in vivo.," *The Journal of neuroscience : the official journal of the Society for Neuroscience*, vol. 27, Dec. 2007, pp. 14231-8.

[2] E.O. Mann and O. Paulsen, "Local Field Potential Oscillations as a Cortical Soliloquy.," *Neuron*, vol. 67, Jul. 2010, pp. 3-5.

[3] R.T. Canolty, K. Ganguly, S.W. Kennerley, C.F. Cadieu, K. Koepsell, J.D. Wallis, and J.M. Carmena, "Oscillatory phase coupling coordinates anatomically dispersed functional cell assemblies," *Proceedings of the National Academy of Sciences*, vol. 107, Sep. 2010, pp. 17356-17361.

[4] L.A. Geddes and C. Hodge, "The retrospectroscope: electrocorticography," *IEEE Engineering in Medicine and Biology Magazine*, vol. 15, 1996, pp. 101-103.

[5] G.S. Brindley and M.D. Craggs, "The electrical activity in the motor cortex that accompanies voluntary movement.," *The Journal of physiology*, vol. 223, May. 1972, p. 28-29.

[6] G. Schalk, "Can Electrocorticography (ECoG) Support Robust and Powerful Brain-Computer Interfaces?," *Frontiers in neuroengineering*, vol. 3, Jan. 2010, p. 9.

[7] J. Kubánek, K.J. Miller, J.G. Ojemann, J.R. Wolpaw, and G. Schalk, "Decoding flexion of individual fingers using electrocorticographic signals in humans.," *Journal of neural engineering*, vol. 6, Dec. 2009, p. 066001 (14 pp).

[8] E.F. Chang, E. Edwards, S.S. Nagarajan, N. Fogelson, S.S. Dalal, R.T. Canolty, H.E. Kirsch, N.M. Barbaro, and R.T. Knight, "Cortical Spatio-temporal Dynamics Underlying Phonological Target Detection in Humans.," *Journal of cognitive neuroscience*, May. 2010.

[9] B. Rubehn, C. Bosman, R. Oostenveld, P. Fries, and T. Stieglitz, "A MEMS-based flexible multichannel ECoG-electrode array.," *Journal of neural engineering*, vol. 6, Jun. 2009, p. 036003.

[10] P. Ledochowitsch, R.J. Felus, R.R. Gibboni, A. Miyakawa, S. Bao, and M.M. Maharbiz, *Fabrication and testing of a large area, high density, parylene MEMS*, IEEE, 2011.

[11] J.E. O'Doherty, M.A. Lebedev, T.L. Hanson, N.A. Fitzsimmons, and M.A.L. Nicolelis, "A brain-machine interface instructed by direct intracortical microstimulation," *Frontiers in Integrative Neuroscience*, vol. 3, 2009, pp. 1-10.

[12] E.S. Boyden, F. Zhang, E. Bamberg, G. Nagel, and K. Deisseroth, "Millisecond-timescale, genetically targeted optical control of neural activity.," *Nature neuroscience*, vol. 8, Sep. 2005, pp. 1263-8.

[13] O. Tuna, Y. Selamet, G. Aygun, and L. Ozyuzer, "High quality ITO thin films grown by dc and RF sputtering without oxygen," *Journal of Physics D: Applied Physics*, vol. 43, Feb. 2010, p. 055402.

[14] M. Boehme and C. Charton, "Properties of ITO on PET film in dependence on the coating conditions and thermal processing," *Surface and Coatings Technology*, vol. 200, Oct. 2005, pp. 932-935.

[15] C.M. Aguirre, S. Auvray, S. Pigeon, R. Izquierdo, P. Desjardins, and R. Martel, "Carbon nanotube sheets as electrodes in organic light-emitting diodes," *Applied Physics Letters*, vol. 88, May. 2006, p. 183104.

[16] S. De, T.M. Higgins, P.E. Lyons, E.M. Doherty, P.N. Nirmalraj, W.J. Blau, J.J. Boland, and J.N. Coleman, "Silver Nanowire Networks as Flexible, Transparent, Conducting Films: Extremely High DC to Optical Conductivity Ratios.," *ACS nano*, vol. 3, Jun. 2009, pp. 1767-1774.

[17] X. Wang, L. Zhi, and K. Müllen, "Transparent, conductive graphene electrodes for dye-sensitized solar cells.," *Nano letters*, vol. 8, Jan. 2008, pp. 323-7.

[18] J. Selvakumaran, M.P. Hughes, J.L. Keddie, and D.J. Ewins, "Assessing biocompatibility of materials for implantable microelectrodes using cytotoxicity and protein adsorption studies," *2nd Annual International IEEE-EMBS Special Topic Conference on Microtechnologies in Medicine and Biology. Proceedings (Cat. No.02EX578)*, 2002, pp. 261-264.

[19] A.S. Bondarenko and G.A. Ragoisha, "EIS Spectrum Analyser."

[20] A. Norlin, "Investigation of interfacial capacitance of Pt, Ti and TiN coated electrodes by electrochemical impedance spectroscopy," *Biomolecular Engineering*, vol. 19, Aug. 2002, pp. 67-71.